Impact of dynamic coupling between relative orbit and attitude on the estimation of relative dynamics of spacecraft

Chaves-Jiménez, A.; Guo, J.; Gill, E.

DOI
10.1016/j.actaastro.2018.08.038

Publication date
2018

Document Version
Accepted author manuscript

Published in
Acta Astronautica

Impact of Dynamic Coupling between Relative Orbit and Attitude on the Estimation of Relative Dynamics of Spacecraft

A. Chaves-Jiménez[a,*], J. Guo[a], E. Gill[a]

[a] *Chair of Space Systems Engineering, Faculty of Aerospace Engineering, Delft University of Technology, Kluyverweg 1, 2629 HS Delft, The Netherlands*

Abstract

In this work the extent to which orbit and attitude sensors may cross-support each other in a joint processing to reduce estimation errors of the relative orbital and attitude dynamics is investigated. In order to do this, an engineering dynamic model taking into account the coupling effects between orbit and attitude dynamics is exploited for estimation purposes. A simple yet common configuration of two spacecraft in an along-track formation flying in low Earth Orbit (LEO) is used as case study, where the atmospheric drag perturbation constitutes the source of coupling. An extended Kalman Filter considering the dynamic coupling between orbital and attitude dynamics is used to estimate the absolute and relative dynamics of the system. It is shown that the coupling leads to higher accuracy estimation results.

Nomenclature

- $\boldsymbol{a}$: vector.
- $\boldsymbol{a}^{\times}$: cross product matrix of a vector $\boldsymbol{a}$.
- $\boldsymbol{a}|_{\mathcal{B}}$: vector $\boldsymbol{a}$ expresed on $\mathcal{B}$ frame.
- $\mathbf{1}_a$: a×a identity matrix.
- $\mathbf{0}_{n\times m}$: n × m zeros matrix.

1. Introduction

Typically, on the estimation of spacecraft dynamics, orbit and attitude dynamics are considered independent from each other [1] [2] [3] [4]. A notable

*Corresponding author
Email addresses: a.chavesjimenez@tudelft.nl (A. Chaves-Jiménez), j.guo@tudelft.nl (J. Guo), e.k.a.gill@tudelft.nl (E. Gill)

exception is the consideration of orbit-attitude coupling for very large spacecraft, by Chodas ([5],[6]) in the early eighties. Here, a dynamic coupling given by both the gravity gradient and the atmospheric perturbation for a single spacecraft with very high effective area (7000 m^2) in a very low orbit (at 250 km altitude) was considered.

Nevertheless, in recent years, the field of spacecraft design is witnessing an emerging paradigm shift from traditional large single satellites to distributed small satellites acting in a collaborative manner. Several types of space missions would be hardly achievable if not for a distributed spacecraft approach. For example, [7] shows 39 formation flying and constellation missions with satellites of less than 10 kg. These applications are increasing the importance of improving the performance of relative dynamics estimation.

On the relative dynamics estimation problem, where the distances to be estimated are of the order of 100 to 2000 m and an expected accuracy of, for example, 0.1 m (3D RSS) for the PRISMA mission([8]), taking into account forces considered negligible for absolute dynamics estimation process may have a real effect on the relative dynamics estimation performance.

For this reason, recent works are taking into account the joint representation of attitude and orbital dynamics for improved guidance, navigation and control performance. For example, in the case of the joint representation of relative dynamics of spacecraft for control purposes, in [9, 10] the gravity-induced mutual coupling between orbital and attitude dynamics is taken into account when solving a spacecraft relative dynamics tracking problem using nonlinear control techniques. In [11] the coupling effect generated by the gravity gradient and the solar pressure is considered in the engineering model of the spacecraft formation control system for a space interferometry mission. Similarly, in [12] it is described how the gravity gradient, solar pressure and atmospheric drag are a source of coupling between attitude and orbital dynamics. Later, this dynamics model is applied for control purposes in [13]. Furthermore, the coupling effect generated by actuation is considered in [14, 15, 16, 17, 18]. The modeling of the coupling of orbit and attitude dynamics for deep space missions is reported in [19, 20]. Also, in [21] and [22], kinematic coupling is described as the orbit-attitude relation perceived when an arbitrary point outside the center of mass is used as the center of the reference frame on the description of spacecraft dynamics. This is done in order to proper describe dynamics as perceived from the real position of sensors on spacecraft structures, but are not related to any perturbation effect dynamic coupling. In [14] and [15] the coupling generated by the alignment of thrusters with respect to the center of mass is taken into account in the model of the dynamics of spacecraft when controlling them for docking purposes. In [16] a general mathematical model is used to represent the coupling generated by both the position of the actuators and the perturbation effect in the estimation of the joint attitude and orbital dynamics. Furthermore, missions where the coupling clearly affect the orbital dynamics, like the ones using solar sails, have attracted increasing attention [17] [18]. In [21] and [22] the relative dynamics of two spacecraft are modeled, with the difference that coupling effect is given due by the fact that the dynamics are represented from a

reference in each spacecraft not located in their center of mass. Practical use of the coupling between attitude and orbital dynamics is proposed by [23], where the differential drag between spacecraft is employed to control their relative distance.

Similarly, the joint relative orbital and attitude dynamics representation has been used for estimation purposes in cases like [24, 25, 26]. In [24], the improvement of the measurement methods, via the use of an optical sensor to provide multiple line-of-sight vectors from one spacecraft to another is used in combination with an Extended Kalman Filter (EKF) to improve the estimation performance. In [25] a " Square-Root sigma-point Kalman Filter" is used in order to improve the estimation of spacecraft relative dynamics. These two papers illustrate two methods for improving the estimation of spacecraft relative dynamics: the use of better measurement approaches, and the use of estimation methods that adapt better to the nonlinear nature of the spacecraft dynamics.

In none of these works has the coupling between orbital and attitude dynamics been taken into account, unlike the cited control application examples. This simplification is typically justified by assuming that the magnitude of this coupling effect is negligible. For this reason, the improvement of the physical modeling of spacecraft dynamics may be seen as a complementary approach to the improvement of the measuring methodology and the use of different estimation methods. Only works such as [27] and [28] take into account the coupling for estimation purposes. In this research, the location of the position sensors on the spacecraft body makes its measurement attitude-dependent.

Nevertheless, to the best of our knowledge, no work has been published yet where the coupling between the attitude and orbital dynamics caused by external perturbations is adopted in spacecraft relative dynamics models to improve their estimation accuracy, in a similar fashion as it has been used for control purposes.

The present paper evaluates how such coupling affects the spacecraft relative position and attitude estimation. This paper presents a similar objective as [5] but this time in the realm of relative pose dynamics. The contribution of this research consists in investigating, using a spacecraft dynamics estimator, to what extent the coupling effects between orbit and attitude dynamics can be advantageously exploited for estimation purposes. The focus of this research is the evaluation of this physical model, and for this reason, a very well known Extended Kalman Filter method is the estimator of choice, due to the fact that its extensive use in spacecraft dynamics estimation, enabling the possibility to use the model here proposed with any other estimators. We use a simple yet common configuration of two spacecraft in along track formation flying in low Earth Orbit (LEO) as a case study. Here the atmospheric drag perturbation constitutes the source of coupling between orbital and attitude absolute and relative dynamics. The proposed system can easily be extended to any amount of spacecraft, and as such, constitutes a tool for the evaluation of how the coupling between relative attitude and orbital dynamics can improve their dynamics estimation performance. It is investigated if the estimation convergence is better when the coupling consideration is taken into account. The approach of this pa-

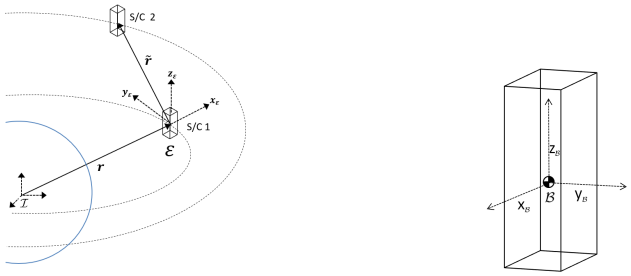

(a) Definition of the Orbital Frame ($\mathcal{E}$)

(b) Definition of the Body Frame ($\mathcal{B}$)

Figure 1: Definition of reference frames

per, where an improvement on the dynamics model is proposed, may be seen as complementary to the approach where new mathematical methods are proposed in order to improve the relative dynamics of spacecraft

2. Spacecraft Absolute and Relative Dynamics Representation

2.1. Definition of Reference Frames

Consider two spacecraft, S/C 1 (chief) and S/C 2 (deputy), orbiting the Earth. Let $\mathcal{I}$ denote an inertial geocentric Cartesian, right-handed coordinate frame [29, p. 28].

Let $\mathcal{E}$ denote an orbital, right-handed, coordinate frame associated with the chief spacecraft (Fig. 1a). In $\mathcal{E}$, the x-axis points towards S/C 1 center of mass, the z-axis points in the direction of the S/C 1 orbital angular momentum, and the y-axis completes the frame [30, p.160]. Finally, let $\mathcal{B}_1$ and $\mathcal{B}_2$ denote spacecraft-centered Cartesian right-handed coordinates frames with origins at the spacecraft centers of mass of S/C 1 and S/C 2 respectively, with the z-axis in the direction of the highest moment of inertia, and the x and y-axes parallel to the area vectors of the faces of the spacecraft (Fig. 1b).

2.2. Dynamics Model Definition

In this section, the dynamics model of the absolute and relative dynamics of spacecraft used in this paper are given, but not derived, for the sake of simplicity. If further information is required about the derivation of these equations, the reader is refered to [29, Ch. 16],[31]. Let $\boldsymbol{r}$ and $\boldsymbol{r}_2$ be the position of the center of mass of S/C 1 and S/C 2, respectively, measured from the center of the Earth, and let $\tilde{\boldsymbol{r}}$ and $\tilde{\boldsymbol{v}}$ denote the relative position and velocity of S/C 2 with respect to S/C 1 , i.e,

$$\tilde{\boldsymbol{r}} = \boldsymbol{r}_2 - \boldsymbol{r} \tag{1}$$

$$\tilde{\boldsymbol{v}} = \frac{d\tilde{\boldsymbol{r}}}{dt} \tag{2}$$

Let $(\tilde{r}_x, \tilde{r}_y, \tilde{r}_z, \tilde{v}_x, \tilde{v}_y, \tilde{v}_z)$ denote the components of $\tilde{\boldsymbol{r}}$ and $\tilde{\boldsymbol{v}}$ in the frame $\mathcal{E}_1$ respectively.

Furthermore, let $\boldsymbol{\omega}$ denote the angular velocity vector of the frame $\mathcal{B}_1$ with respect to $\mathcal{I}$ projected on $\mathcal{B}_1$. For any quaternion, $\boldsymbol{q}$, with vector part $\mathbf{e}$ and scalar part q, let $\Xi(\boldsymbol{q})$ denote the following 4×3 matrix

$$\Xi(\boldsymbol{q}) = \begin{bmatrix} \mathbf{e}^{\times} + q\mathbf{1}_3 \\ -\mathbf{e}^T \end{bmatrix} \tag{3}$$

where $\mathbf{e}^{\times}$ denotes the cross-product matrix

$$\mathbf{e}^{\times} = \begin{bmatrix} 0 & -e_3 & e_2 \\ e_3 & 0 & -e_1 \\ -e_2 & e_1 & 0 \end{bmatrix} \tag{4}$$

and $\mathbf{1}_3$ is the identity matrix in $\mathbb{R}^3$. Let $\boldsymbol{q}$, with vector part $\mathbf{e}$ and scalar part q, denote the quaternion of the rotation from $\mathcal{I}$ to $\mathcal{B}_1$.

Finally, let $\tilde{\boldsymbol{q}} = (\tilde{\boldsymbol{e}}, \tilde{q})$ and $\tilde{\boldsymbol{\omega}}$ denote the relative quaternion and relative angular velocity vector, respectively, of S/C 2 with respect to S/C 1, defined as

$$\tilde{\boldsymbol{q}} = (\boldsymbol{q}_{\mathcal{B}_1})^{-1} * \boldsymbol{q}_{\mathcal{B}_2} \tag{5}$$

$$\tilde{\boldsymbol{\omega}} = \boldsymbol{\omega}_2|_{\mathcal{B}2} - \boldsymbol{\omega}|_{\mathcal{B}2} \tag{6}$$

with $\boldsymbol{q}_{\mathcal{B}_2}$ the quaternion of rotation from $\mathcal{I}$ to $\mathcal{B}_2$ and $\boldsymbol{\omega}_2|_{\mathcal{B}2}$ the rotation rate of $\mathcal{B}_2$ with respect to $\mathcal{I}$ projected in $\mathcal{B}_2$. Here, $\boldsymbol{q}^{-1}$ and $*$ denote the quaternion inverse and composition operations, respectively [29, App. D]. Defining $\boldsymbol{x}$ as the complete state, under the assumption of rigid body rotations around their centers of mass, the absolute and relative orbital and attitude dynamics is governed by the following system of equations [29, Ch. 16],[31]

$$\dot{\boldsymbol{x}} = \begin{bmatrix} \dot{\boldsymbol{r}} \\ \dot{\boldsymbol{v}} \\ \dot{\boldsymbol{q}} \\ \boldsymbol{I}_1 \dot{\boldsymbol{\omega}} \\ \dot{\tilde{\boldsymbol{r}}} \\ \dot{\tilde{\boldsymbol{v}}} \\ \dot{\tilde{\boldsymbol{q}}} \\ \dot{\tilde{\boldsymbol{\omega}}} \end{bmatrix} = \begin{bmatrix} \dot{\boldsymbol{v}} \\ -\frac{\mu}{r^3}\boldsymbol{r} + \boldsymbol{a}_p \\ \frac{1}{2}\,\Xi(\boldsymbol{q})\boldsymbol{\omega} \\ -\boldsymbol{\omega}^{\times}\boldsymbol{I}_1\boldsymbol{\omega} + \boldsymbol{\tau}_1 \\ \tilde{\boldsymbol{v}} \\ p(\boldsymbol{x}) + \boldsymbol{\Delta a_p} \\ \frac{1}{2}\,\Xi(\tilde{\boldsymbol{q}})\,\tilde{\boldsymbol{\omega}} \\ \mathbf{g}(\boldsymbol{\omega}_1, \tilde{\boldsymbol{\omega}}, \tilde{\boldsymbol{q}}) \end{bmatrix} \tag{7}$$

where

$$p(\boldsymbol{x}) = \begin{bmatrix} \frac{\mu}{r^2} - \dfrac{\mu(r + \tilde{r}_x)}{\alpha^3} + 2\Omega_1\tilde{v}_y + \dot{\Omega}_1\tilde{r}_y + \Omega_1^2\tilde{r}_x + \Delta a_{p_x} \\ -\dfrac{\mu\tilde{r}_y}{\alpha^3} - 2\Omega_1\tilde{v}_x - \dot{\Omega}_1\tilde{r}_x + \Omega_1^2\tilde{r}_y + \Delta a_{p_y} \\ -\dfrac{\mu\tilde{r}_z}{\alpha^3} + \Delta a_{p_z} \end{bmatrix}, \tag{8}$$

$$\alpha = \sqrt{(r + \tilde{r}_x)^2 + \tilde{r}_y^2 + \tilde{r}_z^2} \tag{9}$$

$$\Omega_1 = \frac{|\boldsymbol{r}^{\times}\boldsymbol{v}|}{|\boldsymbol{r}|^2}, \tag{10}$$

$$\dot{\Omega}_1 = \frac{(\boldsymbol{r}^{\times}\boldsymbol{v})^T(\boldsymbol{r}^{\times}\dot{\boldsymbol{v}})}{|r|^2|\boldsymbol{r}^{\times}\boldsymbol{v}\|} - 2|\boldsymbol{r}^{\times}\boldsymbol{v}|\frac{\boldsymbol{r}^T\boldsymbol{v}}{|\boldsymbol{r}|^4}, \tag{11}$$

and

$$\begin{aligned}\mathbf{g}(\boldsymbol{x}) = \boldsymbol{I}_2^{-1}\{&\boldsymbol{I}_2\left[\boldsymbol{D}(\tilde{\boldsymbol{q}})\,\boldsymbol{\omega}_1 + \tilde{\boldsymbol{\omega}}\right] \times \left[\boldsymbol{D}(\tilde{\boldsymbol{q}})\,\boldsymbol{\omega}_1 + \tilde{\boldsymbol{\omega}}\right] - \boldsymbol{I}_2\left[\boldsymbol{D}(\tilde{\boldsymbol{q}})\,\boldsymbol{\omega}_1 + \tilde{\boldsymbol{\omega}}\right] \times \tilde{\boldsymbol{\omega}} \\ &-\boldsymbol{I}_2\boldsymbol{D}(\tilde{\boldsymbol{q}})\boldsymbol{I}_1^{-1}\left[(\boldsymbol{I}_1\,\boldsymbol{\omega}_1) \times \boldsymbol{\omega}_1 + \boldsymbol{\tau}_1\right] + \boldsymbol{\tau}_2\big\},\end{aligned} \tag{12}$$

with $\boldsymbol{I}_1, \boldsymbol{I}_2$ the tensors of inertia of the chief and deputy spacecraft around their centers of mass on the frames $\mathcal{B}_1$ and $\mathcal{B}_2$ respectively, and $\boldsymbol{D}(\tilde{\boldsymbol{q}})$ denotes the matrix of the rotation from $\mathcal{B}_1$ to $\mathcal{B}_2$, i.e.:

$$\boldsymbol{D}(\tilde{\boldsymbol{q}}) = (\tilde{q}^2 - \tilde{\boldsymbol{e}}^T\tilde{\boldsymbol{e}})\mathbf{1}_3 + 2\tilde{\boldsymbol{e}}\tilde{\boldsymbol{e}}^T - 2\,q\tilde{\boldsymbol{e}}^{\times}. \tag{13}$$

Here, Ω_1 denotes the absolute value of the angular velocity of $\mathcal{I}$ with respect to $\mathcal{E}$, $\boldsymbol{a}_p$ and $\boldsymbol{\tau}_1$ represent the external force and torque perturbing the dynamics of S/C 1, $\boldsymbol{\Delta a_p}$ represents the differential acceleration affecting the relative orbital dynamics and $\boldsymbol{\tau}_2$ the total perturbation torque acting on the deputy spacecraft. The dynamic coupling described on the next section is produced by some of these external forces and torques.

Equation 7 represents a state space model for the dynamics of spacecraft relative orbital and attitude motions. If we assume in this two-body system that $\|\tilde{\boldsymbol{r}}\| << \|\boldsymbol{r}\|$ and that spacecraft 1 is in a circular orbit, the relative orbital dynamics lead to the well-known Hill-Clohessy-Wiltshire equations [1]. Notice that the number of spacecraft can be arbitrarily increased while using the same modeling equations.

2.3. Description of the Atmospheric Drag as the Source of Coupling between Attitude and Orbital Dynamics

When a satellite is in low-Earth-orbit, the interaction of the upper atmosphere particles with its surface is the cause of atmospheric drag force and torque. This atmospheric perturbation acts directly opposite to the velocity of the satellite motion with respect to the atmospheric flux, producing a deceleration of the satellite [30]. This effect constitutes the strongest non-gravitational perturbation of orbital dynamics missions working at an altitude of around 300 km. This is true for for both absolute [32] and relative orbital dynamics [33].

Typically, the force model considering atmospheric drag use assumes a constant spacecraft effective area. Nevertheless, in reality, unless the satellite is a perfect sphere, or that spacecraft are controlled so that their effective area are

constant, these effective areas change as a function of attitude, meaning that the magnitude of this perturbation on the orbit dynamics is a function of the spacecraft orientation, thus becoming a source of coupling between orbit and attitude dynamics on spacecraft in flight. For the case of atmospheric torque acting on the spacecraft, due to the fact that both the density of the atmosphere and the velocity of the spacecraft depend on the altitude, it also constitutes a source of coupling between orbit and attitude dynamics.

In this section, the effect of the atmospheric drag, considered as the main non-gravitational force acting on spacecraft relative dynamics, is described in the proper reference frames.

The acceleration due to atmospheric drag may be modeled as

$$\boldsymbol{a}_a = -\frac{1}{2}\frac{C_D \rho(\boldsymbol{r})}{m} A_{ef} \boldsymbol{v}_s^2 \hat{\boldsymbol{v}}_s, \tag{14}$$

where C_D the drag coefficient of the S/C, assumed in this case to be the same for all spacecraft surfaces, $\rho(\boldsymbol{r})$ is the atmospheric density, m is the mass of the spacecraft, $\boldsymbol{v}_s$ the velocity of the spacecraft surface with respect to the atmosphere, $\boldsymbol{v}_s = \boldsymbol{v} - \boldsymbol{v}_a$, where $\boldsymbol{v}_a$ is the velocity of the atmosphere.

If a spacecraft is modeled as a number of plane surfaces, the effective area is given by

$$A_{ef} = \sum_{i=1}^{s} A_i (\hat{\boldsymbol{n}}_i^T \cdot \hat{\boldsymbol{v}}_s). \tag{15}$$

where s is equal to the amount of plane surfaces composing the spacecraft,A_i the magnitude of area i amd $\hat{\boldsymbol{n}}_i$ a unit vector perpendicular to area i. The atmosphere is assumed to be spherical and co-rotating with the Earth [34]. In this case, its velocity projection in $\mathcal{I}$ is given by

$$\boldsymbol{v}_a = \boldsymbol{\omega_E} \times \boldsymbol{r}, \tag{16}$$

where $\boldsymbol{\omega_E}$ is the Earth rotation around its own axis.

The torque produced by the atmospheric drag is then given by

$$\boldsymbol{\tau}_a = -\frac{1}{2} C_D \rho(\boldsymbol{r}) \sum_{i=1}^{k} A_i (\hat{\boldsymbol{n}}_i \boldsymbol{v}_s)(\boldsymbol{d}_i \times \boldsymbol{v}_s), \tag{17}$$

with $\boldsymbol{d}_i$ the distance between the center of pressure of area i and the center of mass of the S/C.

2.3.1. Deputy Spacecraft Atmospheric Drag Perturbation

The atmospheric drag force on the deputy spacecraft is given by

$$\boldsymbol{a}_{a,2}|_{\mathcal{E}} = -\frac{1}{2}\frac{C_{D,2}\rho(\boldsymbol{r}_2)}{m_2} \sum_{i=1}^{k} A_{d,i} (\hat{\boldsymbol{n}}_2^T \boldsymbol{v}_{s,2}) \boldsymbol{v}_{s,2} \tag{18}$$

Where r_2 is the position of the deputy spacecraft with respect to the center of Earth, $\boldsymbol{v}_{s,2}$ is the velocity of the spacecraft with respect to the atmosphere. Those values need to be expressed on the $\mathcal{E}$ frame.

Here we have that

$$\boldsymbol{v}_2|_{\mathcal{E}} = \begin{bmatrix} \frac{\boldsymbol{r}^T\boldsymbol{v}}{r} \\ r\left|\frac{\boldsymbol{r}^\times\boldsymbol{v}}{\boldsymbol{r}^2}\right| \\ 0 \end{bmatrix} + \tilde{\boldsymbol{v}} - \boldsymbol{D}|_{\mathcal{E}}^{\mathcal{I}} \left(\boldsymbol{\omega_E}^\times \begin{bmatrix} r+\tilde{r}_x \\ \tilde{r}_y \\ \tilde{r}_z \end{bmatrix} \right). \tag{19}$$

Take again the vectorial representation of the acceleration caused by the atmospheric drag acceleration (eq. 14), in order to derive the expression for the differential drag $\boldsymbol{\Delta a_p}$ affecting the relative dynamics as a function of the states given by eq. 7. For the deputy spacecraft, we have that

$$\begin{aligned} \boldsymbol{r}_2|_{\mathcal{E}} &= \boldsymbol{r}|_{\mathcal{E}} + \tilde{\boldsymbol{r}} & (20)\\ \boldsymbol{v}_{s,2}|_{\mathcal{E}} &= \boldsymbol{v}|_{\mathcal{E}} + \tilde{\boldsymbol{v}} - \boldsymbol{v}_a|_{\mathcal{E}}\,, & (21) \end{aligned}$$

where $\boldsymbol{r}_2$ is the position of S/C 2 with respect to the center of Earth and $\boldsymbol{v}_{s,2}$ is its velocity with respect to the atmosphere. Here $\tilde{\boldsymbol{r}}$ is given in the $\mathcal{E}$frame, but the notation is dropped because the state is defined in this frame already. To determine the relative position of the second spacecraft in $\mathcal{E}$, the definition of this frame leads to $\boldsymbol{r}|_{\mathcal{E}} = [r, 0, 0]^T$, so

$$\boldsymbol{r}_2|_{\mathcal{E}} = \begin{bmatrix} r+\tilde{r}_x \\ \tilde{r}_y \\ \tilde{r}_z \end{bmatrix}. \tag{22}$$

Taking the orbital rate vector of the Chief spacecraft orbit as Ω_1, we obtain

$$\boldsymbol{v}|_{\mathcal{E}} = \begin{bmatrix} \dot{r} \\ r\Omega_1 \\ 0 \end{bmatrix} = \begin{bmatrix} \frac{\boldsymbol{r}^T\boldsymbol{v}}{r} \\ r\left|\frac{\boldsymbol{r}^\times\boldsymbol{v}}{\boldsymbol{r}^2}\right| \\ 0 \end{bmatrix}. \tag{23}$$

To determine the expression for the velocity of the atmosphere projected in $\mathcal{E}$, we use

$$\boldsymbol{v}_a|_{\mathcal{E}} = \boldsymbol{D}|_{\mathcal{E}}^{\mathcal{I}}\,\boldsymbol{v}_a = \boldsymbol{D}|_{\mathcal{E}}^{\mathcal{I}}\,(\boldsymbol{\omega_E}^\times\,\boldsymbol{r}_2|_{\mathcal{E}}) = \boldsymbol{D}|_{\mathcal{E}}^{\mathcal{I}} \left(\boldsymbol{\omega_E}^\times \begin{bmatrix} r+\tilde{r}_x \\ \tilde{r}_y \\ \tilde{r}_z \end{bmatrix} \right), \tag{24}$$

where $\boldsymbol{D}|_{\mathcal{E}}^{\mathcal{I}}$ is the rotation matrix from $\mathcal{I}$ to $\mathcal{E}$. This rotation can easily be obtained using the guidelines described in [35].

So, we obtain

$$\boldsymbol{v}_2|_{\mathcal{E}} = \begin{bmatrix} \frac{\boldsymbol{r}^T\boldsymbol{v}}{r} \\ r\left|\frac{\boldsymbol{r}^{\times}\boldsymbol{v}}{\boldsymbol{r}^2}\right| \\ 0 \end{bmatrix} + \tilde{\boldsymbol{v}} - \boldsymbol{D}|_{\mathcal{E}}^{\mathcal{I}} \left(\boldsymbol{\omega_E}^{\times} \begin{bmatrix} r+\tilde{r}_x \\ \tilde{r}_y \\ \tilde{r}_z \end{bmatrix} \right). \tag{25}$$

Finally, an expression for the vector normal to any area i of spacecraft 2, $\boldsymbol{n}_{2,i}|_{\mathcal{E}}$, is required. This vector is known in the body frame of the deputy spacecraft $\mathcal{B}_2$. The projection of this vector in $\mathcal{E}$ is given by

$$\boldsymbol{n}_{2,i}|_{\mathcal{E}} = \boldsymbol{D}|_{\mathcal{E}}^{\mathcal{I}}\, \boldsymbol{D}^T(\boldsymbol{q})\boldsymbol{D}^T(\tilde{\boldsymbol{q}})\boldsymbol{n}_{2,i}, \tag{26}$$

where $\boldsymbol{n}_{2,i}$ is the normal vector to the area i of S/C 2 projected in $\mathcal{B}_2$.

Replacing 22, 25 and 26 in 14 we have all the elements necessary to express the atmospheric drag acceleration of the second spacecraft using the system states. The differential drag is then expressed as $\boldsymbol{\Delta a_p} = \boldsymbol{a}_{a,2} - \boldsymbol{D}|_{\mathcal{E}}^{\mathcal{I}}\, \boldsymbol{a}_{a,1}$, with $\boldsymbol{a}_{a,1}$ derived in the previous section.

2.3.2. Deputy Spacecraft Atmospheric Drag Torque Perturbation

Take the expression of the atmospheric drag torque (eq. 17). To determine the absolute value of $\boldsymbol{r}_2$, the result from eq. 22 may be used. Also, both the normal vectors to the areas $\hat{\boldsymbol{n}}_i$ and the distance between the center of pressure and the center of mass per area $\boldsymbol{d}_{2,i}$ projected in $\mathcal{B}_2$ are assumed to be known. Given this condition, in order to compute the torque affecting S/C 2 , it is only left to determine the velocity of the deputy spacecraft with respect to the atmosphere projected on $\mathcal{B}_2$. Since

$$\boldsymbol{v}_{s,2}|_{\mathcal{B}2} = \boldsymbol{D}(\tilde{\boldsymbol{q}})\boldsymbol{D}(\boldsymbol{q})\left(\boldsymbol{v} + \tilde{\boldsymbol{v}}|_{\mathcal{I}} - \boldsymbol{v}_a|_{\mathcal{I}}\right), \tag{27}$$

where

$$\tilde{\boldsymbol{v}}|_{\mathcal{I}} = \boldsymbol{D}|_{\mathcal{E}}^{\mathcal{I}}\, \tilde{\boldsymbol{v}} + \Omega|_{\mathcal{I}}^{\mathcal{I}\to\mathcal{E}^{\times}} \boldsymbol{r} = \boldsymbol{D}|_{\mathcal{E}}^{\mathcal{I}}\, \tilde{\boldsymbol{v}} + \frac{(\boldsymbol{r}^{\times}\boldsymbol{v})^{\times}}{r^2}\tilde{\boldsymbol{r}} \tag{28}$$

$$\boldsymbol{v}_{a,2}|_{\mathcal{I}} = \boldsymbol{\omega}_E^{\times}\boldsymbol{r}_2 = \begin{bmatrix} 0 \\ 0 \\ \omega_{Et} \end{bmatrix}^{\times} \left(\boldsymbol{r} + \boldsymbol{D}|_{\mathcal{I}}^{\mathcal{E}}\, \tilde{\boldsymbol{r}}\right), \tag{29}$$

we obtain

$$\boldsymbol{v}_2|_{\mathcal{B}2} = \boldsymbol{D}(\tilde{\boldsymbol{q}})\boldsymbol{D}(\boldsymbol{q}) \left(\boldsymbol{v} + \boldsymbol{D}|_{\mathcal{E}}^{\mathcal{I}}\, \tilde{\boldsymbol{v}} + \frac{(\boldsymbol{r}^{\times}\boldsymbol{v})^{\times}}{r^2}\tilde{\boldsymbol{r}} - \begin{bmatrix} 0 \\ 0 \\ \omega_{Et} \end{bmatrix}^{\times} \left(\boldsymbol{r} + \boldsymbol{D}|_{\mathcal{I}}^{\mathcal{E}}\, \tilde{\boldsymbol{r}}\right) \right) \tag{30}$$

By using eq. 30 in eq. 17 we arrive at the expression of the atmospheric drag torque affecting the deputy spacecraft as a function of the states projected in $\mathcal{B}_2$.

3. States Observation Modeling

Due to the fact that we want to study the impact of coupling on spacecraft relative dynamics estimation, it is necessary to define which measurements will be used on the estimation of the spacecraft states. The most simple assumption that may be done for this purpose would be that "pseudo measurements" of the states are available, this means that it is possible to measure the states directly. Actual sensors exist that provide comparable measurements, for example, GPS or relative GPS for the case of position dynamics.

There are two reasons for this. First of all, a more complex measurement model may interfere with the estimation results, thus not allowing to focus only on the effects of the estimation performance given by the better dynamical model. Second, to reduce to a minimum the sources of error in the results not related to the experiment itself that may appear if a more realistic measurement model is used. Implementation of more sophisticated measurement models to use with the proposed engineering model may be easily done both for an EKF as for any other filtering algorithm to be used with the coupled dynamics model proposed in this paper.

In this paper, the measurement model assumes that the position and attitude states are directly measured, so that

$$\boldsymbol{z}(t) = \begin{bmatrix} \mathbf{1}_3 & \mathbf{0}_{3\times3} & \mathbf{0}_{3\times4} & \mathbf{0}_{3\times3} & \mathbf{0}_{3\times3} & \mathbf{0}_{3\times4} & \mathbf{0}_{3\times3} \\ \mathbf{0}_{4\times3} & \mathbf{0}_{4\times3} & \mathbf{1}_4 & \mathbf{0}_{4\times3} & \mathbf{0}_{4\times3} & \mathbf{0}_{4\times4} & \mathbf{0}_{4\times3} \\ \mathbf{0}_{3\times3} & \mathbf{0}_{3\times3} & \mathbf{0}_{3\times4} & \mathbf{1}_3 & \mathbf{0}_{3\times3} & \mathbf{0}_{3\times4} & \mathbf{0}_{3\times3} \\ \mathbf{0}_{4\times3} & \mathbf{0}_{4\times3} & \mathbf{0}_{4\times4} & \mathbf{0}_{4\times3} & \mathbf{0}_{4\times3} & \mathbf{1}_4 & \mathbf{0}_{4\times3} \end{bmatrix} \begin{bmatrix} \boldsymbol{r} \\ \boldsymbol{v} \\ \boldsymbol{q} \\ \boldsymbol{\omega} \\ \tilde{\boldsymbol{r}} \\ \tilde{\boldsymbol{v}} \\ \tilde{\boldsymbol{q}} \\ \tilde{\boldsymbol{\omega}} \end{bmatrix} + \boldsymbol{\nu}_{\boldsymbol{z}}(t), \tag{31}$$

leading to a direct measurement of the states $\boldsymbol{r}, \boldsymbol{q}, \tilde{\boldsymbol{r}}, \tilde{\boldsymbol{q}}$ with noise $\boldsymbol{\nu}_{\boldsymbol{z}}(t) \sim N(0, R)$, with covariance $R \in \mathbb{R}^{14x14}$ matrix.

4. Extended Kalman Filter

In this work, an extended Kalman Filter (EKF) is used to test the effect of coupling in spacecraft relative dynamics estimation due to its extended use in the spacecraft onboard estimation applications. The EKF may be considered a classic estimator for this applications, and was selected instead of newer proposed estimators, due to the fact that this paper focus on the effect of the use of a more precise dynamics model.

Take an engineering model of the dynamics based on the model of equation 7 and a measurement model based on equation 31

$$\dot{\boldsymbol{x}} = f(\boldsymbol{x}, t) + \boldsymbol{\nu}_x(t), \tag{32}$$
$$\boldsymbol{z}(t) = \boldsymbol{h}(\boldsymbol{x}(t), t) + \boldsymbol{\nu}_{\boldsymbol{z}}(t), \tag{33}$$

where $\boldsymbol{x} \in \mathbb{R}^n$ is the state, $\boldsymbol{z} \in \mathbb{R}^m$ is the output resulting from the measurements, $\boldsymbol{\nu}_x(t) \sim N(0, Q(t))$ the process noise, representing the deviation of the engineering model to the truth model. The linearization of this equation is done around a nominal state $\boldsymbol{x}^*$ and input $\boldsymbol{u}^*$ where $\boldsymbol{x} \in \mathbb{R}$ with $\delta\boldsymbol{x} = \boldsymbol{x} - \boldsymbol{x}^*$ lead us to a discretized perturbation state-variable model associated with the linearized version of the nonlinear system 7 as described in [36].

$$\delta\dot{\boldsymbol{x}} = \boldsymbol{F}_x(\boldsymbol{x}^*, t)\delta\boldsymbol{x} + \boldsymbol{\nu}_x(t), \tag{34}$$
$$\delta\boldsymbol{z} = \boldsymbol{H}_x(\boldsymbol{x}^*, t)\delta\boldsymbol{x} + \boldsymbol{\nu}_{\boldsymbol{z}}(t), \tag{35}$$

where $\boldsymbol{F}_x$ is a $n \times n$ Jacobian matrix and $\boldsymbol{H}_x$ a $m \times n$ matrix ; i.e.

$$\boldsymbol{F}_x(\boldsymbol{x}^*, t) = \begin{bmatrix} \frac{\partial f_1(\boldsymbol{x}^*)}{\partial x_1} & \cdots & \frac{\partial f_1(\boldsymbol{x}^*)}{\partial x_n} \\ \vdots & \ddots & \vdots \\ \frac{\partial f_n(\boldsymbol{x}^*)}{\partial x_1} & \cdots & \frac{\partial f_n(\boldsymbol{x}^*)}{\partial x_n} \end{bmatrix}, \boldsymbol{H}_x(\boldsymbol{x}^*, t) = \begin{bmatrix} \frac{\partial \boldsymbol{h}_1(\boldsymbol{x}^*)}{\partial x_1} & \cdots & \frac{\partial \boldsymbol{h}_1(\boldsymbol{x}^*)}{\partial x_n} \\ \vdots & \ddots & \vdots \\ \frac{\partial \boldsymbol{h}_n(\boldsymbol{x}^*)}{\partial x_1} & \cdots & \frac{\partial \boldsymbol{h}_n(\boldsymbol{x}^*)}{\partial x_n} \end{bmatrix} \tag{36}$$

The implementation of a discrete Extended Kalman Filter (EFK) for the nonlinear system of equations 32 and 33 based on the linearization of equations 34 and 35 is based on two processes: prediction and measurement update.

4.1. Prediction

Prediction uses the last estimated state $\hat{\boldsymbol{x}}(k, k)$ to obtain a prediction of the value of the state $\boldsymbol{x}$ in time $k + 1$ by using the analytical model of the state. The predicted state is called $\hat{\boldsymbol{x}}(k + 1, k)$

$$\hat{\boldsymbol{x}}(k + 1, k) = \hat{\boldsymbol{x}}(k, k) + \int_{t_k}^{t_k+1} \boldsymbol{f}(\hat{\boldsymbol{x}}(k + 1, k), \boldsymbol{u}^*(t), t)dt. \tag{37}$$

4.2. Measurement Update

Correction uses the measurements of the state in time $k + 1$ to update the prediction and finally arrive at the estimated state $\hat{\boldsymbol{x}}(k+1, k+1)$ and its covariance matrix $\boldsymbol{P}(k+1, k+1)$. The weight of the the prediction and the correction is determined by the gain matrix $\boldsymbol{K}(k + 1)$.

$$\hat{\boldsymbol{x}}(k + 1, k + 1) = \hat{\boldsymbol{x}}(k + 1, k) + \boldsymbol{K}(k + 1)\left\{\boldsymbol{z}(k + 1) - \boldsymbol{h}(\hat{\boldsymbol{x}}(k + 1, k), k + 1\right. \tag{38}$$
$$\boldsymbol{P}(k + 1, k + 1) = \left[\boldsymbol{1}_n - \boldsymbol{K}(k + 1)\boldsymbol{H}_{\boldsymbol{x}}(k + 1, k)\right] \boldsymbol{P}(k + 1, k) \tag{39}$$

where

Initial Conditions.		
Spacecraft	**S/C 1**	**S/C 2**
Position (km)	$[300km + R_E, 0, 0]$	$(300 + R_E)[\cos\theta_2, \sin\theta_2, 0]$
Velocity (km/s)	$[0, 7.7142, 0]$	$7.7142[-\sin\theta_2, \cos\theta_2, 0]$
Attitude quaternion	$[0, 0, 0, 1]$	$[0, 0, 0, 1]$
Rotation rate for the rotating case (rad/s)	$[0, pi/18, 0]$	$[0, 0, \pi/18]$
Initial along-track separation (R_A)	1000 km	
Spacecraft mechanical characteristics.		
Mass (m)	3.6 kg	3.6 kg
Inertia matrix ($\boldsymbol{I}$)	$\begin{bmatrix} 0.055 & 0 & 0 \\ 0 & 0.055 & 0 \\ 0 & 0 & 0.017 \end{bmatrix}$ kg m^2	$\begin{bmatrix} 0.055 & 0 & 0 \\ 0 & 0.055 & 0 \\ 0 & 0 & 0.017 \end{bmatrix}$ kg m^2
Drag coefficient (C_D)	2.3	2.3

Table 1: Configuration of the dynamics of the system under study.

$$\boldsymbol{K}(k+1) = \boldsymbol{P}(k+1,k)\left[\boldsymbol{H_x}(k+1,k)\boldsymbol{P}(k+1,k)\boldsymbol{H_x}^T(k+1,k) + \boldsymbol{R}(k+1)\right]^{-1} \quad (40)$$

$$\boldsymbol{P}(k+1,k) = \boldsymbol{\Phi}(t,t_0)\boldsymbol{P}(k,k)\boldsymbol{\Phi}^{\boldsymbol{T}}(t,t_0) + \boldsymbol{Q}(k+1,k) \quad (41)$$

$$\boldsymbol{\Phi}(t,t_0) = e^{\boldsymbol{F}_x(t-t_0)} \quad (42)$$

and $\boldsymbol{R}(k+1), \boldsymbol{Q}(k+1,k)$ and $\boldsymbol{H_x}(k+1,k)$ are the linearized versions of $\boldsymbol{R}(t), \boldsymbol{Q}(t)$ and $\boldsymbol{H}_x(t)$. Please be aware that the equations including here do not include an input function. For the most general form of the equation and details about the derivation of the linearized version of the $\boldsymbol{R}(k+1), \boldsymbol{Q}(k+1,k)$ and $\boldsymbol{H_x}(k+1,k)$ we refer the reader to [36].

5. Scenario

Take the two spacecraft system orbiting Earth with dynamics described in equation 7. These two spacecraft follow a circular equatorial orbit with an initial altitude of 300 km in an along-track configuration with a relative distance of 1000 km. An equatorial orbit is selected in order to avoid taking into account the J_2 effects on the dynamics model. This altitude is selected because in this orbit a strong signal of the coupling due to the atmospheric drag is obtained. Its use is justified by its applicability in distributed space systems (DSS) missions ranking from Earth-observation to gravity missions. This orbit is of use also for future DSS missions that may avoid debris by best placed in very low orbits. The drag coefficients (C_D) of both spacecraft are equal and assumed to have the same dimensions of the ones used in the simulation of the formation flying mission proposed by TU Delft in the framework of the QB50 mission [32].

The parameters used in the scenario are given on Table 1.

It is assumed that the atmospheric density is known, and is given by its values at solar radiation maximum (see [37]).

The accuracy of the pseudo-measurements is defined on table 2.

In order to demonstrate the effect of coupling, two EKF are used: one that includes the coupling dynamics in the engineering model described by equation

Sensor	Noise variance
Relative position	$\pm 100\ m$
Attitude quaternion	± 0.1

Table 2: Sensors accuracy

Configuration	size (cm^3)
CubeSat (3U)	30 x 10 x 10
Large Spacecraft	240 x 80 x 80

Table 3: Test cases area configuration for the spacecraft

7. This estimator is called for now on the "Coupled Estimator". Another estimator was implemented for its use in comparison purposes. In this one, the engineering model assumes that the area of the spacecraft are constant, and equal to the largest possible facing area of both satellites. This estimator is called here the "Uncoupled Estimator".

Two different kind of satellite, by size, are used on this research. The first kind of spacecraft is a 3-unit Cubesat, one of the smallest forms proposed for cooperative missions, for example in the QB-50 mission [32]. These satellites have a 30x10x10 cuboid form. For comparison purposes, another "large spacecraft" is used. The size of the "large spacecraft" is defined as a cuboid with the same ratio between sides of the CubeSat configuration, while at the same time having a size comparable to a large spacecraft used for formation flying missions. With this purpose, the "large spacecraft" is set up as a cuboid where each side is 8 times larger than every side of the CubeSat configuration. With this expansion, the "large spacecraft" size is similar in size to the spacecraft used for the Grace mission (length = 312.2 cm, height = 72 cm, bottom width = 194.2 cm, top width = 69.3 cm) [38]. For reference, their sizes are described on table 3.

The process noise to be used in the implementation of the EKF is fundamental for the proper performance of both estimators. The noise matrix to be

Table 4: Process noise configuration for the coupled and uncoupled estimator.

$n_{\boldsymbol{r}}$	10^{-9}	$n_{\tilde{\boldsymbol{r}}}$	10^{-9}
$n_{\boldsymbol{v}}$	10^{-9} (Calibrated)	$n_{\tilde{\boldsymbol{v}}}$	10^{-9} (Calibrated)
$n_{\boldsymbol{q}}$	10^{-7}	$n_{\tilde{\boldsymbol{q}}}$	10^{-7}
$n_{\boldsymbol{\omega}}$	10^{-5}	$n_{\tilde{\boldsymbol{\omega}}}$	10^{-5}

used in the engineering model $\boldsymbol{Q}(k)$ is given as

$$\boldsymbol{Q}(k+1) = \left[\begin{array}{cccc:cccc} \boldsymbol{Q}_{\boldsymbol{r}} & \mathbf{0}_{3\times3} & \mathbf{0}_{3\times4} & \mathbf{0}_{3\times3} & \mathbf{0}_{3\times3} & \mathbf{0}_{3\times3} & \mathbf{0}_{3\times4} & \mathbf{0}_{3\times3} \\ \mathbf{0}_{3\times3} & \boldsymbol{Q}_{\boldsymbol{v}} & \mathbf{0}_{3\times4} & \mathbf{0}_{3\times3} & \mathbf{0}_{3\times3} & \mathbf{0}_{3\times3} & \mathbf{0}_{3\times4} & \mathbf{0}_{3\times3} \\ \mathbf{0}_{4\times3} & \mathbf{0}_{4\times3} & \boldsymbol{Q}_{\boldsymbol{q}} & \mathbf{0}_{4\times16} & \mathbf{0}_{3\times3} & \mathbf{0}_{3\times3} & \mathbf{0}_{3\times4} & \mathbf{0}_{3\times3} \\ \mathbf{0}_{3\times3} & \mathbf{0}_{3\times3} & \mathbf{0}_{3\times3} & \boldsymbol{Q}_{\boldsymbol{\omega}} & \mathbf{0}_{3\times3} & \mathbf{0}_{3\times3} & \mathbf{0}_{3\times4} & \mathbf{0}_{3\times3} \\ \hdashline \mathbf{0}_{3\times3} & \mathbf{0}_{3\times3} & \mathbf{0}_{3\times4} & \mathbf{0}_{3\times3} & \boldsymbol{Q}_{\tilde{\boldsymbol{r}}} & \mathbf{0}_{3\times3} & \mathbf{0}_{3\times4} & \mathbf{0}_{3\times3} \\ \mathbf{0}_{3\times3} & \mathbf{0}_{3\times3} & \mathbf{0}_{3\times4} & \mathbf{0}_{3\times3} & \mathbf{0}_{3\times3} & \boldsymbol{Q}_{\tilde{\boldsymbol{v}}} & \mathbf{0}_{3\times4} & \mathbf{0}_{3\times3} \\ \mathbf{0}_{3\times3} & \mathbf{0}_{3\times3} & \mathbf{0}_{3\times4} & \mathbf{0}_{3\times3} & \mathbf{0}_{4\times3} & \mathbf{0}_{4\times3} & \boldsymbol{Q}_{\tilde{\boldsymbol{q}}} & \mathbf{0}_{4\times3} \\ \mathbf{0}_{3\times3} & \mathbf{0}_{3\times3} & \mathbf{0}_{3\times4} & \mathbf{0}_{3\times3} & \mathbf{0}_{3\times3} & \mathbf{0}_{3\times3} & \mathbf{0}_{3\times4} & \boldsymbol{Q}_{\tilde{\boldsymbol{\omega}}} \end{array}\right] \tag{43}$$

where $\boldsymbol{Q}_{\alpha} = n_{\alpha}^2 \mathbf{1}_3$ with $\alpha = \{\boldsymbol{r}, \boldsymbol{v}, \boldsymbol{q}, \boldsymbol{\omega}, \tilde{\boldsymbol{r}}, \tilde{\boldsymbol{v}}, \tilde{\boldsymbol{q}}, \tilde{\boldsymbol{\omega}}\}$ and $\boldsymbol{Q}_{\beta} = n_{\alpha}^2 \mathbf{1}_4$ with $\beta = \{\boldsymbol{q}, \tilde{\boldsymbol{q}}\}$. The values for each one of these process noises used for this simulation are given in table 4.

For spacecraft estimation purposes, incorporating the non-modeled perturbation effects to the dynamics model as part of the process noise is a common practice (this is done for example in [24]). For this reason, in order to prove that the "Coupled Estimator" leads to a better performing estimation, the magnitude of the velocity process noise of the uncoupled estimator is adjusted until the estimation reaches its best performance. In this way, the process noise is used to simulate the atmospheric drag for the "Uncoupled Estimator". This is the reason why the velocity process noise is indicated on table 4 as "Calibrated". The best possible uncoupled estimator is defined as the one that leads to the lowest average estimation error after five orbits. The estimation error $\Delta\tilde{\boldsymbol{r}}_u$ is defined as the error between the real dynamics and the dynamics predicted by the uncoupled Estimator.

In order to configure the magnitude of the velocity noise, the following procedure is used:

1. The initial value for both $n_{\boldsymbol{v}}, n_{\tilde{\boldsymbol{v}}}$ is set to be the largest magnitude of the atmospheric drag force $\boldsymbol{a}_a$ at the evaluating altitude. For example, on the 300 km orbit propagation, for the largest spacecraft, the largest absolute value of the atmospheric drag force was calculated to be $9.9170 \cdot 10^{-4}$ N.

2. The estimator is propagated for five orbits.
3. The magnitude of $\Delta\tilde{\boldsymbol{r}}_u$ is calculated.
4. The magnitudes of $n_{\boldsymbol{v}}, n_{\tilde{\boldsymbol{v}}}$ is incremented and decremented in steps of 10% of their initial value until the minimum value of the average of $\Delta\tilde{\boldsymbol{r}}_u$ for the fifth orbit is obtained. For example, in this case, for the incremented process noise, we use $n_{\boldsymbol{v}} = 10.9087$, that constitutes 10 % more than the initial process noise use.
5. This increment and decrement continues until the lowest value for $\Delta\tilde{\boldsymbol{r}}_u$ is found. For this example, the value of the process noise that lead to the lowest error was $6.9419 \cdot 10^{-4}$ (a 30 % decrement from the initial value).

Hence, the calibration procedure is based on the minimization of $\Delta\tilde{\boldsymbol{r}}_u$ via the calibration of the velocities process noise. This calibration is done every time the area or the altitude is changed.

The objective of this is to compare the Coupled Estimator with the best possible uncoupled estimator. With this, it is shown that even in the best possible assumption of the perturbation as a white-Gaussian noise, the Coupled estimator shows a better performance in terms of convergence and precision.

6. Results and Analysis

In this section, it will be shown how the model taking into account the coupling between relative position and attitude impacts the performance of the estimation of orbital relative dynamics. For this, two variables are evaluated: the change in the spacecraft effective area and the change in the spacecraft set altitude. Take into account the fact that the mass of the spacecraft is not changed for any of the simulations, the change of area may be interpreted here also as the change of the area-mass ratio.

Here, the improvement on the estimation results is shown via the difference on the estimation error between the coupled and the uncoupled estimator, and also by showing the accumulated variance of both estimators, via the accumulative effect of the estimation convergence. This simulation is propagated five orbits, showing clearly the best convergence of the coupled estimator.

6.0.1. Scenario 1: Variation of the spacecraft effective area

In order to evaluate the effect of the effective area of the spacecraft in formation, this work uses four different area configurations, all with a rectangular form, starting from a 3-unit Cubesat configuration (30x10x10 cm), one of the smallest area configurations proposed for formation flying missions. This base configuration was selected due to its popular use in spacecraft constellation projects like Planet Labs constellation [39] and One Web [40]. From here, areas are incremented to observe the relation between its variation and the estimation performance. The areas used are summarized on table 5.

Results using the smallest satellite (a 3 unit Cubesat configuration) are shown in figure 2, and with the largest in 3, both in a circular orbit with an

Area Configuration	Area $[cm^3]$
1	30 x 10 x 10
2	60 x 20 x 20
3	120 x 30 x 30
4	240 x 40 x 40

Table 5: Variation of the area of the spacecraft for sensitivity analysis

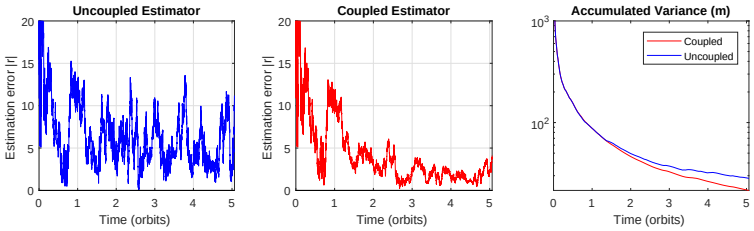

Figure 2: Relative position estimation results for a 2-spacecraft formation with 3-unit Cubesat configuration.

altitude of 300 km. Here it is shown that even in the smallest spacecraft area case, coupled estimator outperforms the "Best Uncoupled Estimator".

Now, in figure 4 it is shown how the variance after the fifth orbit differs for the uncoupled and the coupled case, and its variability with the spacecraft area, as a parameter of the performance of the estimator with respect to the spacecraft area. For reference, the values shown in this figure are the values after five orbits of the "accumulated variance" value shown on figures 3 and 4. Here, as expected, it is clear that with a larger area, the difference between the coupled and the uncoupled estimator is higher. With an increment in the order of 32 between the smallest and the largest area, the difference between variances for the smallest spacecraft is of 10.849 m, but for the largest spacecraft it is of 28.651 m, a factor of three.

Here it is shown that even for the smallest spacecraft evaluated, the coupled estimator shows an improvement on the estimation performance. These differences are significant for most Earth Observation missions proposed in present times.

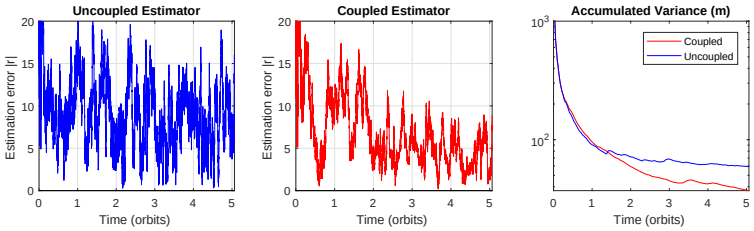

Figure 3: Relative position estimation results for the large spacecraft case.

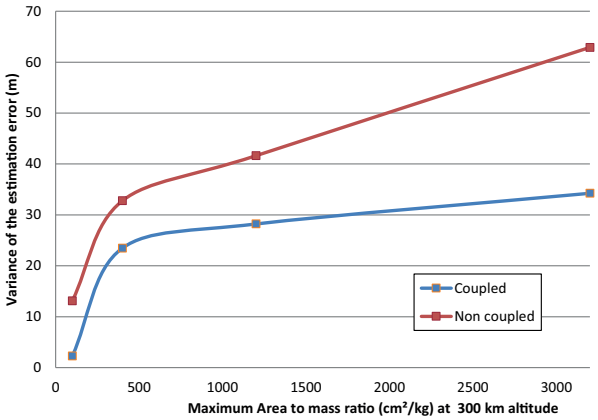

Figure 4: Variance of the error after five orbit with respect to the spacecraft area at a 300 km altitude.

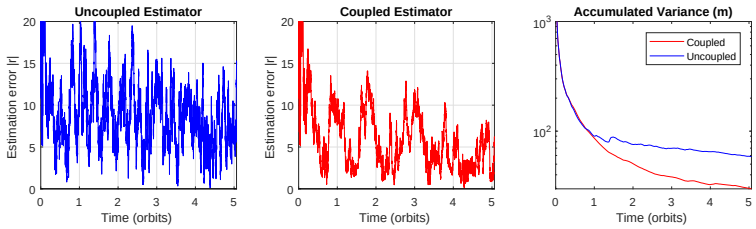

Figure 5: Variance of the error after five orbit at 350 km altitude.

6.0.2. Scenario 2: Variation of the spacecraft altitude

In order to see the effect of the coupled consideration for different attitudes, the orbits of two-satellite, both with the largest spacecraft area (Area 4 of table 5) are propagated in circular orbits with different altitudes. The estimation performance of this configuration in a 300 km altitude orbit was already illustrated in the first scenario in figure 3.

Take now the results of increasing the spacecraft altitude, shown in figure 5 for 350 km altitude and in figure 6 for 650 km altitude. Both figures shown that even for a 650 km orbit, the coupled estimator lead to non-negligible improvements on the estimation performance of the dynamics.

Now, for comparison purposes, take figure 7 showing the result of the final value of the accumulated variance after five orbits for the coupled and the uncoupled estimator with respect to the altitude. It is clear that even at a 650 km altitude, the coupled estimator leads to better results. Nevertheless, the difference between both estimator considerably diminishes at this altitude.

The main variable affecting here the estimation performance is the atmospheric density, that changes from a value of $3.96 \cdot 10^{-11}\ kg/m^3$ for the 300 km altitude to $2.64 \cdot 10^{-13}\ kg/m^3$, a magnitude 250 times higher for the former

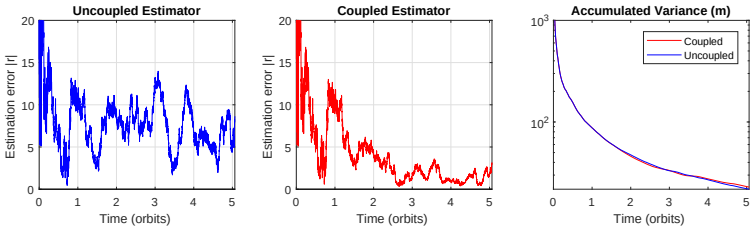

Figure 6: Variance of the error after five orbit at 650 km altitude.

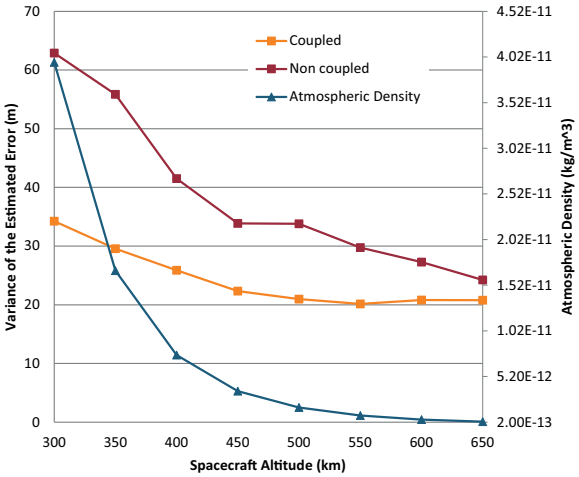

Figure 7: Variance of the error after five orbit with respect to the altitude.

compared to the latter. Nevertheless, this is not the only variable affecting the estimation performance. For reference, the variation of the atmospheric density is also illustrated on figure 7. At a lower altitude, the velocity to remain in a circular orbit is higher, hence the effect of the atmospheric perturbation further increased. For this, it is very difficult to compute the direct relation between the physical variables and the increment in performance due to the altitude changes. The accumulated variance after five orbits for the 300 km altitude is of 34.247 m for the coupled case, and of 62.898 m for the uncoupled case, a difference of almost 30 meters in variation. Nevertheless, for the 650 km altitude evaluation, the variance is of 20.7728 m for the coupled case and 24.230 m for the uncoupled case. With this, it may be concluded that fundamentally for all cases here evaluated, the difference between estimators is not significant beyond 700 km altitude.

7. Conclusions and Future Work

This works shows how the coupling between orbit and attitude dynamics caused by the atmospheric drag force and torque improves the estimation of relative dynamics of spacecraft. For this, the effectiveness of the "Coupled estimator" (an estimator considering such physical effect) is shown.

For comparison purposes, another estimator where the perturbation was simulated using only white-Gaussian noise, is used. Using white Gaussian noise to simulate the perturbation effect is a common practice in spacecraft dynamics estimation. Due to the fact that it may be argued that the selection of the magnitude of this noise may affect the validity of the comparison, the magnitude of the white-Gaussian noise was adjusted until the lowest average error after five orbits was obtained on the estimation process. Even under this condition, the "Coupled Estimator" shows a better estimation performance.

For a case of a very low orbit, a 300 km altitude orbit, even with two CubeSat flying in a along-track configuration, the improvement shown by the use of the coupled estimator is significant, leading to an improvement of 6.951 m in the average position estimation compared to the "best uncoupled estimator".

Changes in estimation performance are even observed for altitudes of as much as 650 km, where for a 240x40x40 cm spacecraft, an improvement of 3.457 m in the average of the error in the estimation of relative position is shown. Nevertheless, when altitudes over 700 km are used in our experiments, the difference in negligible, as expected.

This work leads then to a first estimation of an approximate rank of cases coupling may be considered to improve the estimation performance of relative dynamics of spacecraft using a orbit-attitude model closer to reality, and a method to be applied to different formation flying configurations. Take into account that this work makes use of the nonlinear orbit and attitude dynamics equations, and because of this, is not limited to circular or near-circular orbits, as it may be, for example, if the Clohessy-Wiltshire equations were used. The use of more complex models has been restricted in the past due to computation constraints, but the latest improvements in electronics computing performance,

both in speed and in power consumption, lead to the possibility of using more complex spacecraft dynamics models in on-board spacecraft computers with no additional risk.

Future work may take into account other spacecraft formation flying configuration with different densities, elliptic orbits, and other effects, like the gravity gradient in different relative pose configurations, the diurnal effect of the atmosphere, as well as the use of other estimation techniques that provide better operation performance when spacecraft nonlinear dynamics are used.

References

[1] W. Clohessy, R. Wiltshire, Terminal guidance system for satellite rendezvous, Journal of the Aerospace Sciences 27 (9) (1990) 653–658.

[2] J. Tschauner, Elliptic orbit rendezvous, AIAA Journal 6 (5) (1967) 87–101.

[3] C. McInnes, Autonomous Ring Formation for a Planar Constellation of Satellites, AIAA Journal of Guidance, Control and Dynamics 5 (18) (1995) 1215–1217.

[4] K. Alfriend, H. Yan, S. Vadali, Nonlinear Considerations in Satellite Formation Flying, in: Proceedings of the 2002 AIAA/AAS Astrodynamics Specialist Conference, Monterey CA, 2002.

[5] P. Chodas, Combined satellite attitude and orbit determination with dynamic coupling, in: Astrodynamics Conference, 1982. doi:10.2514/6.1982-1419.

[6] P. W. Chodas, Combined orbit/attitude determination for low-altitude satellites, Ph.D. thesis, Institute of Aerospace Studies, University of Toronto (1986).

[7] S. Bandyopadhyay, R. Foust, G. P. Subramanian, S.-J. Chung, F. Y. Hadaegh, Review of Formation Flying and Constellation Missions Using Nanosatellites, Journal of Spacecraft and Rockets 53 (3) (2016) 1–12. doi:10.2514/1.A33291.

[8] E. Gill, O. Montenbruck, S. D'Amico, Autonomous formation flying for the prisma mission, Journal of Spacecraft and Rockets 44 (3) (2007) 671–681.

[9] H. Pan, V. Kapila, Adaptive nonlinear control for spacecraft formation flying with coupled translational and attitude dynamics, in: Decision and Control, 2001. Proceedings of the 40th IEEE Conference on, Vol. 3, IEEE, 2001, pp. 2057–2062.

[10] H. Pan, H. Wong, V. Kapila, Output feedback control for spacecraft with coupled translation and attitude dynamics, in: 43th IEEE Conference on Decision and Control, 2004.

[11] S. Gaulocher, Modeling the Coupled Translational and Rotational Relative Dynamics for Formation Flying Control, in: AIAA Guidance, Navigation and Control Conference, 2005, pp. 1–6.

[12] R. Kristiansen, E. Grotli, P. J. Nicklasson, J. T. Gravdahl, A model of relative translation and rotation in leader-follower spacecraft formations, Modeling, Identification and Control 28 (1) (2007) 3–13.
URL http://www.ingentaconnect.com/content/nfa/mic/2007/00000028/00000001/art00002

[13] R. Kristiansen, P. J. Nicklasson, J. T. Gravdahl, Spacecraft Coordination Control in 6DOF: Integrator Backstepping vs Passivity-Based Control, Automatica (44) (2008) 2896–2901.

[14] W. Lu, Y. Geng, X. Chen, F. Zhang, Relative position and attitude coupled control for autonomous docking with a tumbling target, International Journal of Control and Automation 4 (4) (2011) 1–22.

[15] L. Sun, W. Huo, Robust adaptive relative position tracking and attitude synchronization for spacecraft rendezvous, Aerospace Science and Technology 41 (2015) 28–35.

[16] F. Zhang, G. Duan, M. Hou, Integrated relative position and attitude control of spacecraft in proximity operation missions with control saturation, International Journal of Innovative Computing, Information and Control 8 (5B) (2012) 3537–3551.

[17] S. Gong, H. Baoyin, J. Li, Coupled attitude–orbit dynamics and control for displaced solar orbits, Acta Astronautica 65 (5) (2009) 730–737.

[18] M. Huo, J. Zhao, S. Xie, N. Qi, Coupled Attitude-Orbit Dynamics and Control for an Electric Sail in a Heliocentric Transfer Mission., PloS one 10 (5) (2015) e0125901. doi:10.1371/journal.pone.0125901.
URL http://www.ncbi.nlm.nih.gov/pubmed/25950179

[19] G. Misra, M. Izadi, A. Sanyal, D. Scheeres, Coupled orbit-attitude dynamics and relative state estimation of spacecraft near small solar system bodies, Advances in Space Research.

[20] A. J. Knutson, D. Guzzetti, K. C. Howell, M. Lavagna, Attitude responses in coupled orbit-attitude dynamical model in earth–moon lyapunov orbits, Journal of Guidance, Control, and Dynamics (2015) 1–10.

[21] S. Segal, P. Gurfil, Effect of kinematic rotation-translation coupling on relative spacecraft translational dynamics, Journal of Guidance, Control and Dynamics 32 (3).

[22] D. Lee, G. Vukovich, Kinematically coupled spacecraft relative motion without attitude synchronization assumption, Aerospace Science and Technology 45 (2015) 316–323.

[23] B. Kumar, A. Ng, K. Yoshihara, A. De Ruiter, Differential drag as a means of spacecraft formation control, Aerospace and Electronic Systems, IEEE Transactions on 47 (2) (2011) 1125–1135. doi:10.1109/TAES.2011.5751247.

[24] S. Kim, J. Crassidis, Y. Cheng, Kalman filtering for relative spacecraft attitude and position estimation, Journal of Guidance, Control, and Dynamics 30 (1) (2007) 133–143.
URL http://dnc.tamu.edu/drjunkins/yearwise/2005/conference/gnc_2005_formation_estimation_visnav.pdf

[25] X. Tang, J. Yan, D. Zhong, Square-root sigma-point Kalman filtering for spacecraft relative navigation, Acta Astronautica 66 (5-6) (2010) 704–713. doi:10.1016/j.actaastro.2009.08.016.
URL http://linkinghub.elsevier.com/retrieve/pii/S0094576509004275

[26] Y. Xing, X. Cao, S. Zhang, H. Guo, F. Wang, Relative position and attitude estimation for satellite formation with coupled translational and rotational dynamics, Acta Astronautica 67 (34) (2010) 455 – 467. doi:10.1016/j.actaastro.2010.04.002.
URL http://www.sciencedirect.com/science/article/pii/S0094576510001190

[27] L. Cao, X. Chen, A. K. Misra, A novel unscented predictive filter for relative position and attitude estimation of satellite formation, Acta Astronautica 112 (2015) 140–157.

[28] L. Cao, H. Li, Novel Cubature Predictive Filter for Relative Position and Attitude Estimation of Satellite Formation Considering J2, Journal of Aerospace Engineering 29 (2) (2016) 04015049. doi:10.1061/(ASCE)AS.1943-5525.0000545.
URL http://ascelibrary.org/doi/10.1061/{%}28ASCE{%}29AS.1943-5525.0000545

[29] J. R. Wertz (Ed.), Spacecraft Attitude Determination and Control, D. Reidel, Dordrecht, The Netherlands, 1984.

[30] O. Montenbruck, E. Gill, Satellite orbits: models, methods and applications, Springer, 2005.

[31] K. Alfriend, S. R. Vadali, P. Gurfil, J. How, L. Breger, Spacecraft Formation Flying: Dynamics, Control and Navigation, Vol. 2, Butterworth-Heinemann, 2009.

[32] E. Gill, P. Sundaramoorthy, J. Bouwmeester, B. Zandbergen, R. Reinhard, Formation flying within a constellation of nano-satellites: The qb50 mission, Acta Astronautica (0) (2012) –. doi:10.1016/j.actaastro.2012.04.029.

URL http://www.sciencedirect.com/science/article/pii/S0094576512001440

[33] S. D'Amico, Autonomous Formation Flying in Low Earth Orbit, TU Delft, Delft University of Technology, 2010.

[34] W. Zhong, P. Gurfil, Online estimation of mean orbital elements with control inputs, in: Proceedings of the EuroGNC 2013, 2nd CEAS Specialist Conference on Guidance, Navigation & Control, Delft University of Technology, 2013.

[35] A. Noureldin, T. Karamat, J. Georgy, Basic navigational mathematics, reference frames and the earths geometry, in: Fundamentals of Inertial Navigation, Satellite-based Positioning and their Integration, Springer Berlin Heidelberg, 2013, pp. 21–63. doi:10.1007/978-3-642-30466-8_2.
URL http://dx.doi.org/10.1007/978-3-642-30466-8_2

[36] J. M. Mendel, Lessons in estimation theory for signal processing, communications, and control, Pearson Education, 1995.

[37] W. J. Larson, J. R. Wertz, Space mission analysis and design, Tech. rep., Microcosm, Inc., Torrance, CA (US) (1992).

[38] eoPortal Directory, Grace (gravity recovery and climate experiment), accessed: 2017-11-03.
URL https://directory.eoportal.org/web/eoportal/satellite-missions/g/grace

[39] D. Butler, Many eyes on earth, Nature 505 (7482) (2014) 143–144.

[40] M. Rice, J. R. Samson Jr, J. Haque, Space-based networking using cubesat technologies, in: 33rd AIAA International Communications Satellite Systems Conference and Exhibition, 2015, p. 4317.